# Crystallization patterns of monomers with a nearest-neighbor interaction on a multilayered semi-infinite square lattice

Alain J. Phares and Francis J. Wunderlich

*Department of Physics, Mendel Hall, Villanova University, Villanova, Pennsylvania 19085-1699*

(Received 27 February 1995)

The absorption of an external monomer gas in a square lattice of $L$ layers, infinite in one direction and finite ($M$ sites) in the other, is studied with a finite nearest-neighbor repulsion energy $V_{11} < 0$. In a physical system, the monomer chemical potential $\mu_1$ is determined by the external gas pressure. For a temperature below $(-V_{11}/5k_B)\log_{10}e$ the curves of entropy $S$ versus lattice coverage $\theta_1$ exhibit two cusps for $L = 1$ and 2, and three cusps for $L = 3$, at $S = 0$. Crystallization pattern analysis at the cusps leads, in terms of $M$ and $L$, to exact expressions of $\theta_1$ and the number $\theta_2$ of nearest neighbors per site which are linear in $1/M$. Setting $M = \infty$ yields, for $L = 1$ and 2, one cusp at $(\theta_1 = \frac{1}{2}, \theta_2 = 0)$, and for $L = 3$, two cusps at $(\theta_1 = \frac{1}{2}, \theta_2 = 0)$ and at $(\theta_1 = \frac{5}{6}, \theta_2 = \frac{5}{3})$. The change in $\mu_1$ required to unlock the structural ordering is shown to be proportional to $V_{11}$. Other features of the system below the critical temperature reported above are also discussed.

PACS number(s): 02.50.$-$r, 05.50.$+$q, 05.70.$-$a

## I. INTRODUCTION

Lattice models have been investigated for seven decades with one of the most cited early models being the Lenz and Ising model of ferromagnetism [1]. The development of statistical thermodynamics has greatly benefited from the study of these models [2]. Here, we study the equilibrium adsorption of nonoverlapping monomer species on a surface having $N$ sections of $M$ equally spaced sites, in the thermodynamic limit $N = \infty$, with nearest-neighbor interaction. The study also includes absorption of monomers in two and three layers ($L=2$ and 3) of $M \times N$ arrays of sites. For a lattice infinite in both directions ($N = \infty$, $M = \infty$) and with $L=1$, 2, and 3, the behavior of the system is obtained using the method of Fowler and Rushbrooke [3], that is, by extrapolation of the results for increasing values of $M$. For example, Kramers and Wannier [4] used this method to investigate the thermal properties of the Ising model with no external field, and similar extrapolations were also made in the case of the infinite nearest-neighbor monomer repulsion (nearest-neighbor exclusion), referred to as the *hard-square* model [5]. Our model goes beyond the hard-square model in that we allow for finite nearest-neighbor interactions, as in the study of physical adsorption isotherms for planar and cylindrical $M \times N$ lattices done by Hock and McQuistan [6]. These authors compared results for the two types of lattices, and observed anomalous particle densities along the free edges of the planar lattice, in a certain range of nearest-neighbor particle-particle interaction energies, and for various values of $M$. Our analysis considers planar lattices beyond the energy range investigated in Ref. [6], and further includes the study of absorption in two and three layers of planar lattices.

The monomers in the lattice (lattice gas) come from an external gas. At equilibrium, the external gas pressure determines each monomer's chemical potential $\mu_1$. Monomers in the lattice do not interact with the monomers in the external gas; but each one has an interaction energy $V_{10}$ with the lattice, and an interaction energy $V_{11}$ with a monomer occupying a nearest-neighbor site. The absolute temperature $T$ of the system is maintained constant, while $\mu_1$ is varied by adjusting the external gas pressure. Thus, the model is a lattice gas with an externally produced chemical potential, which is similar to the Ising model in an external magnetic field [7]. Our system is a two-state system, that is, a lattice site may be either occupied or unoccupied, and we have interactions only between nearest-neighbor occupied sites. The two absolute activities of the lattice gas related to the monomer lattice and to the monomer-monomer nearest-neighbor interactions are

$$x_1 = \exp\left[\frac{\mu_1 + V_{10}}{k_B T}\right] = 10^{\bar{\mu}_1}, \quad x_2 = \exp\left[\frac{V_{11}}{k_B T}\right] = 10^{\bar{\mu}_2},$$

(1)

respectively. Here $k_B$ is Boltzmann's constant, and $\bar{\mu}_1$ and $\bar{\mu}_2$ are dimensionless parameters conveniently chosen for conducting numerical calculations. In the thermodynamic limit, and for different lattice widths $M$, we obtain the entropy of the lattice gas with adsorption taking place on one layer ($L=1$), and absorption taking place in two ($L=2$) or three ($L=3$) layers. Extrapolations of the result to $M = \infty$ follow as indicated above. For a given species of monomers, interaction energies $V_{10}$ and $V_{11}$ are fixed. With the system held at a constant temperature $T$, $x_2$ is fixed and so is $\bar{\mu}_2$. Changes in the external gas pressure produce changes in the chemical potential $\mu_1$ and, therefore, changes in $\bar{\mu}_1$. Thus, an entropy isotherm curve is generated by varying $\bar{\mu}_1$ keeping $\bar{\mu}_2$ fixed. Entropy curves for different values of $\bar{\mu}_2$ correspond to either

different isothermal curves for the same monomer species (given values of $V_{10}$ and $V_{11}$), or to different species of monomers at the same temperature, or both.

We observe the existence of cusps in the entropy curves, as was reported to be the case with dimer species [8]. The information obtained is crucial for the investigation of a mixture of monomers and dimers [9] which is a first step in developing a model of chemical reactions on a surface (heterogeneous catalysis) [10]. As an example, we could think of carbon monoxide adsorbed on Ni(100) which is the preferred catalyst for methanation (Fischer-Tropsch hydrocarbon synthesis). At low coverages of carbon monoxide, two upright species exist, assigned to on-top (monomer) and bridge positions (dimer) [10].

## II. TRANSFER MATRIX

Computing time is greatly reduced when the transfer matrix is recursively constructed, and a slightly different technique than the one used in Ref. [6] is required. In Ref. [8], we showed how it is possible to obtain the recursive construction of the transfer matrix for a system of nonoverlapping dimers on a planar $M \times N$ lattice, with nearest-neighbor interaction. This technique is easily extended to species of different shapes and to other types of lattices as well. In the following, any matrix with upper index $L$ and lower index $M$ is of rank $2^{LM}$ and refers to a semi-infinite lattice of $L$ planar layers of width $M$, and we follow the same procedure for the recursive construction of the transfer matrix, $T_M^L$, for nonoverlapping monomers on $L$ layers of planar $M \times N$ lattices. For a given number $L$ of layers, the construction is based on a diagrammatic short-cut, as demonstrated in Ref. [8].

Figure 1 shows the diagrams needed for a one-layer lattice. Two kinds of block matrices have to be considered, $T_M^1$ and $P_M^1$, and the diagrammatic recursive constructions of $T_M^1$ and $P_M^1$ are shown in Figs. 1(a) and 1(b), respectively. Each matrix is divided into four block matrices, expressed as the product of activities and $T_M^1$ and $P_M^1$. The entries of the block matrices are occupational configurations of a section of the lattice having $M$ sites, with each site represented by a square cell. When the occupation of a cell is arbitrary it is left blank, when it is constrained to be vacant it is marked by a circle, and when it is constrained to be occupied by a monomer it is marked by a filled circle. The *horizontal* and *vertical* entries are associated with the occupational configurations of the *first* and *second* of the $N$ sections of $M$ cells making up the $M \times N$ lattice, respectively. In Fig. 1(a), the horizontal entries are the configurations of the *first section* corresponding to the two possible occupations of the cell at the *right edge* of the lattice, leaving the remaining cells with arbitrary occupation. Similarly, the vertical entries of Fig. 1(a) are the configurations of the *second section* of $M$ cells, with the cell at the *right edge* being either vacant or occupied, leaving the remaining cells with arbitrary occupation. Thus, as shown in Ref. [8], the block matrices are obtained by considering the matching of the occupational configurations of the horizontal and vertical entries. The (11) and (21) block matrices correspond to having a vacancy (activity equal to 1) in the cell at the
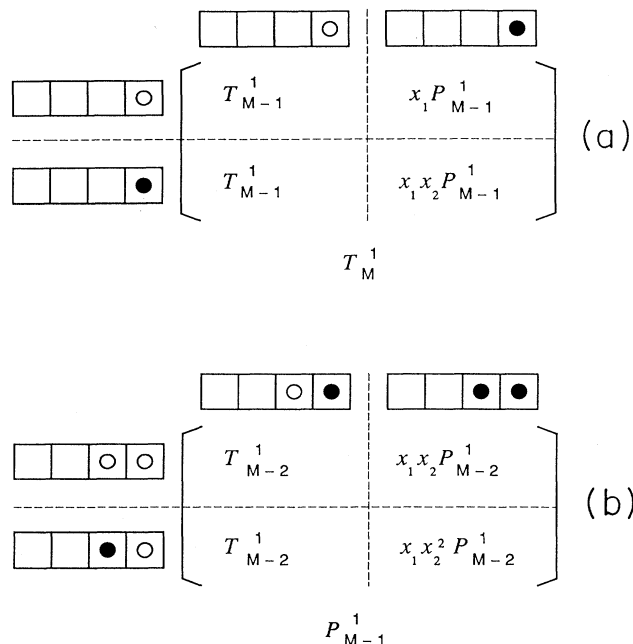


FIG. 1. Recursive construction of the transfer matrix $T_M^1$ for one layer of $M \times N$ lattice sites.

right edge of the second section of the lattice, thus creating either a vacancy-vacancy or a vacancy-monomer nearest neighbor with the cell at the right edge of the first section. No interaction energies are associated with these types of nearest neighbors, and, in both cases, the absolute activity is 1. Following Ref. [8], the corresponding (11) and (21) block matrices are both $T_{M-1}^1$. On the other hand, the (12) and (22) block matrices of Fig. 1(a) correspond to having a monomer in the cell at the right edge of the second section (activity equal to $x_1$), thus creating either a vacancy-monomer (activity equal to 1), or a monomer-monomer (activity equal to $x_2$) nearest neighbor with the cell at the right edge of the first section. A new matrix $P_{M-1}^1$ is exhibited and the corresponding block matrices are of the form $x_1 P_{M-1}^1$ and $x_1 x_2 P_{M-1}^1$. Matrix $P_{M-1}^1$ occurs when requiring a vacancy-monomer or a monomer-monomer occupation in the cells at the right edge of the first and second sections, leaving the remaining $M-1$ cells with an arbitrary occupation. Thus, either of these configurations can be used to generate the recursive construction of $P_{M-1}^1$. Figure 1(b) exhibits this construction with the choice of the vacancy-monomer combination. Thus, the block matrix entries of Fig. 1(b) restrict the occupation of the cell second from the right edge of either the first or second section of the lattice, leaving the occupation of the remaining $M-2$ cells arbitrary. The block matrices of Fig. 1(b) are obtained in a manner similar to that considered in Fig. 1(a), and show that $P_{M-1}^1$ is recursively related to $T_{M-2}^1$ and to $P_{M-2}^1$.

The same technique applies to any number $L$ of layers. The block matrix entries involve the first and second of the $N$ sections of the lattice with $L$ layers, each containing $M$ cells. In each of these two sections, we consider all

possible occupations of the $L$ cells at the right edge, leaving the occupation of the remaining cells arbitrary. Thus, the transfer matrix $T_M^L$ is divided into $4^L$ block matrices. For two layers, Fig. 2 shows the necessity of introducing three additional matrices, $P_M^2$, $Q_M^2$, and $U_M^2$. The transfer matrix $T_M^2$ is related to $P_{M-1}^2$, $Q_{M-1}^2$, $U_{M-1}^2$,

and $T_{M-1}^2$. The constructions of $P_M^2$, $Q_M^2$, and $U_M^2$ are similar to that of $P_M^1$ and are not presented. The additional matrices may also be shown to be related recursively to $T$ only, so that, in the final analysis, $T$ is recursively related to itself. We report the final results for one and two layers, namely:

$$T_M^1 = \begin{bmatrix} T_{M-1}^1 & x_1 T_{M-1}^1 \alpha_{M-1}^1 \\ T_{M-1}^1 & x_1 x_2 T_{M-1}^1 \alpha_{M-1}^1 \end{bmatrix}, \quad \alpha_M^1 = \begin{bmatrix} 1 & 0 \\ 0 & x_2 \end{bmatrix} \otimes I_{M-1}^1 ; \tag{2a}$$

$$T_M^2 = \begin{bmatrix} T_{M-1}^2 & x_1 T_{M-1}^2 \alpha_{M-1}^2 & x_1 T_{M-1}^2 \beta_{M-1}^2 & x_1^2 x_2 T_{M-1}^2 \gamma_{M-1}^2 \\ T_{M-1}^2 & x_1 x_2 T_{M-1}^2 \alpha_{M-1}^2 & x_1 T_{M-1}^2 \beta_M^2 & x_1^2 x_2^2 T_{M-1}^2 \gamma_{M-1}^2 \\ T_{M-1}^2 & x_1 T_{M-1}^2 \alpha_{M-1}^2 & x_1 x_2 T_{M-1}^2 \beta_{M-1}^2 & x_1^2 x_2^2 T_{M-1}^2 \gamma_{M-1}^2 \\ T_{M-1}^2 & x_1 x_2 T_{M-1}^2 \alpha_{M-1}^2 & x_1 x_2 T_{M-1}^2 \beta_{M-1}^2 & x_1^2 x_2^3 T_{M-1}^2 \gamma_{M-1}^2 \end{bmatrix}, \tag{2b}$$

with

$$\alpha_M^2 = \begin{bmatrix} 1 & 0 \\ 0 & 1 \end{bmatrix} \otimes \begin{bmatrix} 1 & 0 \\ 0 & x_2 \end{bmatrix} \otimes I_{M-1}^2 ,$$

$$\beta_M^2 = \begin{bmatrix} 1 & 0 \\ 0 & x_2 \end{bmatrix} \otimes \begin{bmatrix} 1 & 0 \\ 0 & 1 \end{bmatrix} \otimes I_{M-1}^2 , \tag{2c}$$

$$\gamma_M^2 = \begin{bmatrix} 1 & 0 \\ 0 & x_2 \end{bmatrix} \otimes \begin{bmatrix} 1 & 0 \\ 0 & x_2 \end{bmatrix} \otimes I_{M-1}^2 .$$

Here $I$ refers to the identity matrix whose rank is specified by its indices, and the operation $\otimes$ is the Kronecker product of matrices. The initial conditions are

$$T_0^L = \alpha_0^L = \beta_0^L = \gamma_0^L = 1 . \tag{2d}$$

It should be noted that the transfer matrix must satisfy the symmetry property, $T_M^L = T_L^M$, a property which has been used to check the validity of our numerical calculations.

### III. THERMODYNAMIC QUANTITIES

In the thermodynamic limit, the partition function is given by $T_M^L$'s largest eigenvalue [8], $R(x_1, x_2)$, raised to the power $1/LM$. In turn, the fraction $\theta_1$ of lattice sites occupied by monomers, and $\theta_2$, the number of nearest neighbors per site, are given as

$$\theta_1 = \frac{x_1}{LMR} \frac{\partial R}{\partial x_1}, \quad \theta_2 = \frac{x_2}{LMR} \frac{\partial R}{\partial x_2} . \tag{3}$$

The entropy per site divided by Boltzmann's constant (hereafter referred to as entropy) is

$$S = \frac{1}{LM} \ln R - \theta_1 \ln x_1 - \theta_2 \ln x_2 . \tag{4}$$

A normalized quantity, $\theta_2'$, representing the fraction of the maximum number of nearest neighbors is

$$\theta_2' = \frac{LM}{3LM - L - M} \theta_2 . \tag{5}$$

All the numerical calculations were done on the Cray C90 computer at the Pittsburgh Supercomputing Center. For given values of $\bar{\mu}_2$, we varied $\bar{\mu}_1$, and evaluated $\theta_1$, $\theta_2$, and $S$ for $M=1$ to 8 with $L=1$, $M=1$ to 5 with $L=2$, and $M=1$ to 4 with $L=3$. An extremum of the entropy curve is obtained when its partial derivative with respect to $x_1$ at that point is zero, i.e.,

$$\frac{\partial S}{\partial x_1} = -\frac{\partial \theta_1}{\partial x_1} \ln x_1 - \frac{\partial \theta_2}{\partial x_1} \ln x_2$$

$$= -\frac{\partial \theta_1}{\partial x_1} \ln[x_1 x_2^{(\partial \theta_2/\partial \theta_1)_{x_2}}] = 0 . \tag{6a}$$

This occurs when, at that point, either the coverage of the lattice is an extremum, or

$$x_1 x_2^{(\partial \theta_2/\partial \theta_1)_{x_2}} = 1 \Longrightarrow \bar{\mu}_1 = -\left[\frac{\partial \theta_2}{\partial \theta_1}\right]_{x_2} \bar{\mu}_2 . \tag{6b}$$
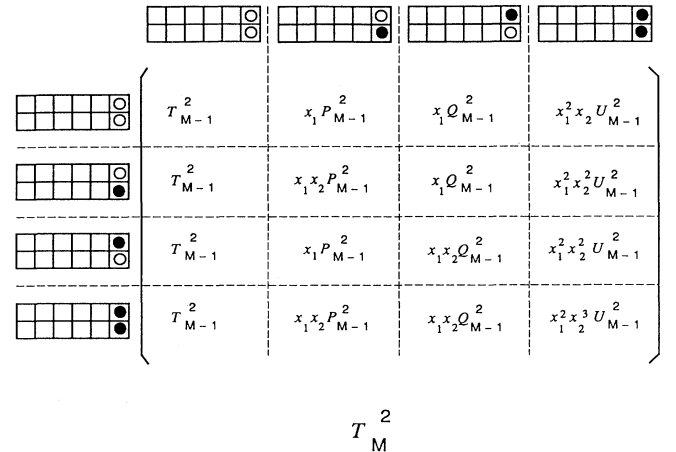
FIG. 2. Recursive construction of the transfer matrix $T_M^2$ for two layers of $M \times N$ lattice sites.

## IV. COMPARISON BETWEEN THE FEATURES IN ONE DIMENSION AND THOSE OF ONE, TWO, AND THREE LAYERS OF PLANAR LATTICES

The one-dimensional problem $(M=1, L=1)$ has been solved [1,2] and is recovered using the general matrix formulation presented above. The transfer matrix is of rank 2, and its largest eigenvalue is

$$R = \tfrac{1}{2}(1+x_1x_2+\sqrt{\Delta}), \quad \Delta=4x_1+(1-x_1x_2)^2, \quad (7)$$

from which $\theta_1$ and $\theta_2$ follow:

$$\theta_1= \frac{x_1}{R\sqrt{\Delta}}[1+x_2(R-1)], \quad \theta_2'=\theta_2= \frac{x_1x_2}{R\sqrt{\Delta}}(R-1) . \quad (8)$$

We consider the behavior of the entropy at sufficiently low temperature with repulsive nearest-neighbor interaction.

A limiting case is that of the hard-square model with nearest-neighbor exclusion and for which $\theta_2=0$ and $x_2=0$, for which $x_1$ and $S$ are obtained in terms of $\theta_1$ as

$$x_1= \frac{\theta_1(1-\theta_1)}{(1-2\theta_1)^2} , \quad (9)$$

$$S = -\theta_1\ln\theta_1+(1-\theta_1)\ln(1-\theta_1)$$
$$-(1-2\theta_1)\ln(1-2\theta_1) . \quad (10)$$

Furthermore, the entropy maximizes at $x_1=1$ with

$$\theta_1= \frac{\sqrt{5}-1}{2\sqrt{5}}, \quad S=\ln\left[\frac{1+\sqrt{5}}{2}\right] , \quad (11)$$

and the maximum possible coverage is $1/2$ with zero entropy.

For $x_2$ positive but very small compared to 1 (finite nearest-neighbor repulsion at low temperature), we consider the range of values of $x_1$ for which $x_1x_2$ is first very large and then very small compared to 1. In the first case, we set $x_1x_2^2=\alpha^2$, and find

$$R \approx \frac{\sqrt{x_1}}{2}[\alpha+\sqrt{4+\alpha^2}], \quad \theta_2= \frac{\alpha}{\sqrt{4+\alpha^2}} , \quad (12)$$

$$\theta_1= \frac{\alpha+\sqrt{4+\alpha^2}}{2\sqrt{4+\alpha^2}} \Longrightarrow \theta_2=2\theta_1-1 . \quad (13)$$

The minimum possible coverage is $\tfrac{1}{2}$, with $\theta_2=0$, $\alpha=0$, and the entropy is zero. Otherwise, the entropy is given in terms of $\alpha$ as

$$S =\ln\left[\frac{\alpha+\sqrt{4+\alpha^2}}{2}\right] - \frac{\alpha\ln\alpha}{\sqrt{4+\alpha^2}} , \quad (14a)$$

and in terms of the coverage $\theta_1$ as

$$S =\theta_1\ln\theta_1-(1-\theta_1)\ln(1-\theta_1)-(2\theta_1-1)\ln(2\theta_1-1) . \quad (14b)$$

It maximizes at

$$\alpha^2=x_1x_2^2=1, \quad S=\ln\left[\frac{1+\sqrt{5}}{2}\right],$$
$$\theta_1= \frac{1+\sqrt{5}}{2\sqrt{5}}, \quad \theta_2'= \frac{1}{\sqrt{5}} . \quad (15)$$

In the second case, $x_1x_2$ is negligible compared to 1, and the discussion is equivalent to setting $x_2=0$. The entropy is given by Eq. (10) and is valid in the region $0\le\theta_1\le\tfrac{1}{2}$. Making the substitution $\theta_1\to1-\theta_1$, Eq. (14b) becomes Eq. (10), proving that, for repulsive nearest-neighbor interaction and at relatively low temperature, the entropy as a function of the coverage is made of two arches, symmetric with respect to the axis $\theta_1=\tfrac{1}{2}$, and forming a cusp at this point, where the entropy is zero. The apices of the arches occur at coordinates given by Eqs. (11) and (15). The plot of $\theta_2$ versus $\theta_1$ is made of two segments, $\theta_2=0(0\le\theta_1\le\tfrac{1}{2})$ and $\theta_2=2\theta_1-1$ $(\tfrac{1}{2}\le\theta_1\le1)$, which meet at $\theta_1=\tfrac{1}{2}$. Many of these features are also found in the infinite two-dimensional lattice gas with one and two layers.

The general problem does not have a closed form analytic solution and is investigated numerically. The constant $\bar{\mu}_2$ curves of $\theta_2'$ versus $\theta_1$ and of $S$ versus $\theta_1$ are similar to those obtained for the system of nearest-neighbor interacting dimers [8]. Figure 3 provides data for $L=1$, $M=3$ and 5; Fig. 4 provides data for $L=2$, $M=3$, and $L=3$, $M=3$. Data for several values of $\bar{\mu}_2$ are shown only in the case $L=1$, $M=3$ (Fig. 3) to exhibit the general features in a wide range of the energy parameter. The other graphs refer to the nearest-neighbor repulsion at sufficiently low temperature (limiting curves).

The data points in the plot $\theta_2'$ versus $\theta_1$ fall inside a polygon. For $\bar{\mu}_2>0$, the curve rapidly approaches $\theta_2'=\theta_1$, the upper boundary of the polygon. For $\bar{\mu}_2<-5$, the curve rapidly approaches the lower boundary which is made of several segments meeting at vertices corresponding to cusps in the entropy curves.

For $S$ versus $\theta_1$, the upper boundary is the $\bar{\mu}_2=0$ curve, an arch with an apex occurring at $\bar{\mu}_1=0$. For $\bar{\mu}_2>0$, the apex of the arch rapidly approaches zero as $\bar{\mu}_2$ increases. In Fig. 3, only a few points are shown with $\bar{\mu}_2>0$. For $\bar{\mu}_2<0$, there is a progressive deformation of the arch. For $\bar{\mu}_2<-5$, the curves become hardly distinguishable and approach a boundary made of several arches meeting at cusps where the entropy is zero. In that limit, and for $L=1$ and 2 (Figs. 3 and 4), the first maximum (state $a$) is followed by the first cusp (state $b$), a second maximum (state $c$), a second cusp (state $d$), and a third maximum (state $e$). For three layers (Fig. 4), the third maximum (state $e$) is followed by a third cusp (state $f$) and a fourth maximum (state $g$). The thermodynamic quantities associated with states $a$ through $g$ will be labeled accordingly.

## V. CUSPS AND MAXIMA OF THE ENTROPY

Monomer and dimer [8] lattice gases share common features. Excluding $\theta_1=0$ and 1, a cusp in the entropy curve always occurs when the entropy is zero. However, for a dimer lattice gas, we have observed cases where

cusps occur for nonzero entropy [8]. We also note that, at a given coverage, the entropy of the lattice gas is a minimum when the number of nearest neighbors per site is also a minimum, corresponding to a point on the lower boundary, in the plot $\theta_2$ versus $\theta_1$, and in the plot of $S$ versus $\theta_1$. Thus, at a given coverage, we search for those configurations having the minimum number of nearest neighbors; if their number is finite, the corresponding entropy of the system must be zero, and we have a cusp.

The analysis of cusp configurations for one, two, and three layers is presented in Figs. 5, 6, and 7, respectively. In these figures, each drawing represents one possible configuration for a given lattice width $M$ and a given set of values of coverage $\theta_1$ and nearest neighbor per site $\theta_2$. As explained in the captions, a drawing gives the occupational configuration in any two consecutive sections of the lattice. The only other possible occupational configurations for the given values of $M$, $\theta_1$, and $\theta_2$ are obtained by symmetry, and, since they are finite in number, the entropy of the system is zero. There are two sets of configurations with zero entropy for one and two layers, and three sets in the case of three layers, corresponding to definite crystallization patterns of the lattice gas.

In all cases, the first set corresponds to $\theta_1 = \frac{1}{2}$ and $\theta_2 = 0$. For a lattice width $M$, the second set of zero entropy configurations occurs at

$$L = 1: \quad \theta_1 = \frac{1}{2} + \left\lceil \frac{1}{M} \right\rceil, \quad \theta_2 = 3 \left\lceil \frac{1}{M} \right\rceil;$$

$$L = 2: \quad \theta_1 = \frac{1}{2} + \left\lceil \frac{1}{M} \right\rceil, \quad \theta_2 = 4 \left\lceil \frac{1}{M} \right\rceil;$$

$$L = 3: \quad \theta_1 = \frac{1}{2} + \frac{2}{3} \left\lceil \frac{1}{M} \right\rceil, \quad \theta_2 = \frac{8}{3} \left\lceil \frac{1}{M} \right\rceil.$$

A third set exists only for three layers of width $M$ given by

$$L = 3: \quad \theta_1 = \frac{5}{6} + \frac{1}{3} \left\lceil \frac{1}{M} \right\rceil, \quad \theta_2 = \frac{5}{3} + \left\lceil \frac{1}{M} \right\rceil.$$

This analysis is exact, and the crystallization patterns at finite nearest-neighbor repulsion and low temperature are exactly obtained for any value of $M$, and $L = 1$, 2, and 3. Therefore their limits at $M = \infty$ (infinite two-dimensional
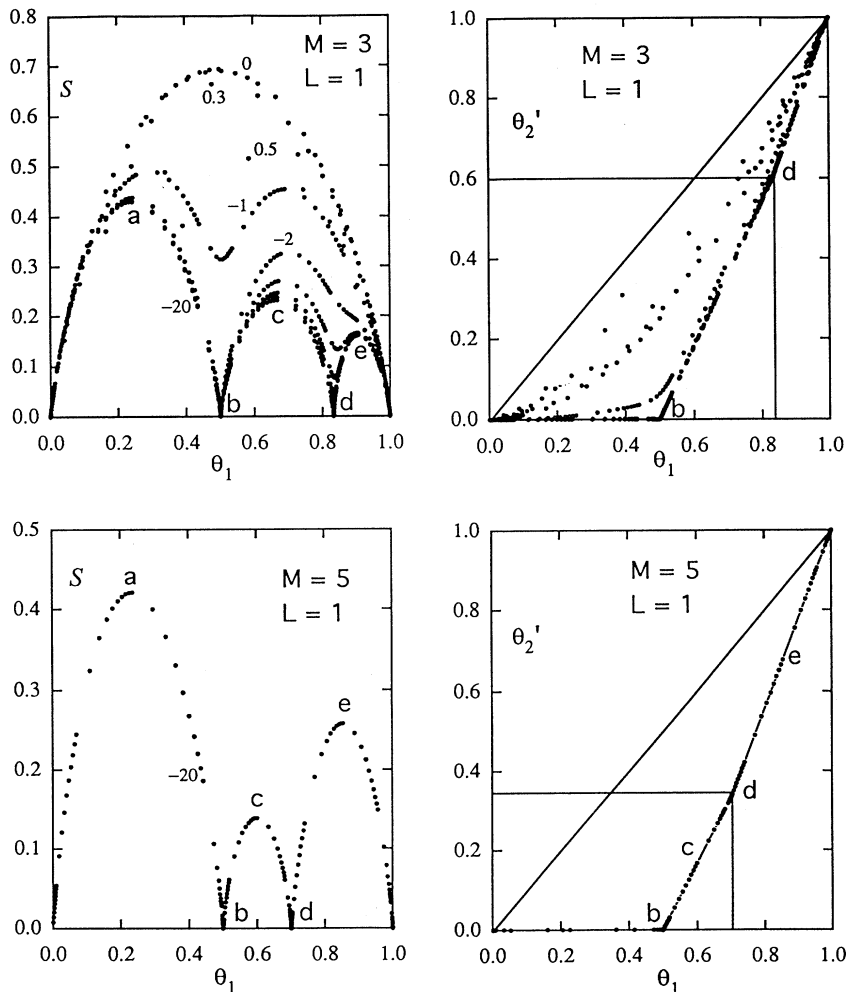


FIG. 3. Labeled constant $\bar{\mu}_2$ curves of entropy $S$, and fraction of the maximum number of nearest neighbors $\theta_2'$ vs the coverage $\theta_1$, for $L = 1$ and $M = 3$, 5. For $M = 5$, we only plot the data at the lower boundary.

lattice, up to three layers) are also exact, and we predict one crystallization at $\theta_1 = \frac{1}{2}$ and $\theta_2 = 0$ for all three layers, as in one dimension, and another at $\theta_1 = \frac{5}{6}$ and $\theta_2 = \frac{5}{3}$ for the infinite three-layer lattice.

To verify that no crystallization patterns are present other than those obtained theoretically, numerical calculations were performed with three distinct computer programs to treat one, two, and three layers. Since a lattice with $L$ layers and width $M$ is topologically the same as that with $M$ layers and width $L$, we were able to numerically check our results by comparing the overlapping cases. Calculations were carried out with an accuracy exceeding 12 significant figures (Figs. 3 and 4), and confirmed the existence of no other cusps than those presented in Figs. 5, 6, and 7. To be sure that this continues to be the case for values of $M$ exceeding the computer's capability, we conducted the following analysis.

To obtain an extrapolation of the data for the infinitely wide lattice of one, two, and three layers, we plot the values of $S$, $\theta_1$, and $\theta_2'$ versus $1/M$, states $a$ through $g$. Linearity at the cusps (states $b$, $d$, $f$) for $\theta_1$ and $\theta_2$ as functions of $1/M$ is exact (see the equations in Figs. 5, 6,

and 7) and was verified numerically. At all other states, linearity is achieved with great accuracy.

Figure 8 shows the entropy for one, two, and three layers at $a$, $e$, and $g$ versus $1/M$ ($g$ exists only for $L = 3$). Linearity is achieved with correlation coefficients better than 0.999 97. Linear extrapolation of the data leads to the results presented in Table I, for the infinite lattice with one, two, and three layers. The configurations of Figs. 5, 6, and 7 show that, as width $M$ becomes infinite, the first and second cusps, states $b$ and $d$, merge at $\frac{1}{2}$ coverage. Thus, the entropy at $c$, which is the maximum between these two cusps, should reach zero in that limit. Figure 9 is the plot of the entropy at $c$ versus $1/M$. Linear regression for $S$ on the infinite lattice using the data for $L = 1$ and 2, which match perfectly, yields the value of $-3.3 \times 10^{-6}$. Linear extrapolation of the only two data points available for $L = 3$ gives for $S$ the value of $-3.0 \times 10^{-8}$. This confirms our theoretical prediction and, at the same time, gives an order of magnitude of the accuracy involved in the linear extrapolation. Figure 10 presents the plots of the coverage of the lattice at $a$, $c$, $e$, and $g$ versus $1/M$, for one, two, and three layers. The results of the linear extrapolation to the infinite lattice are
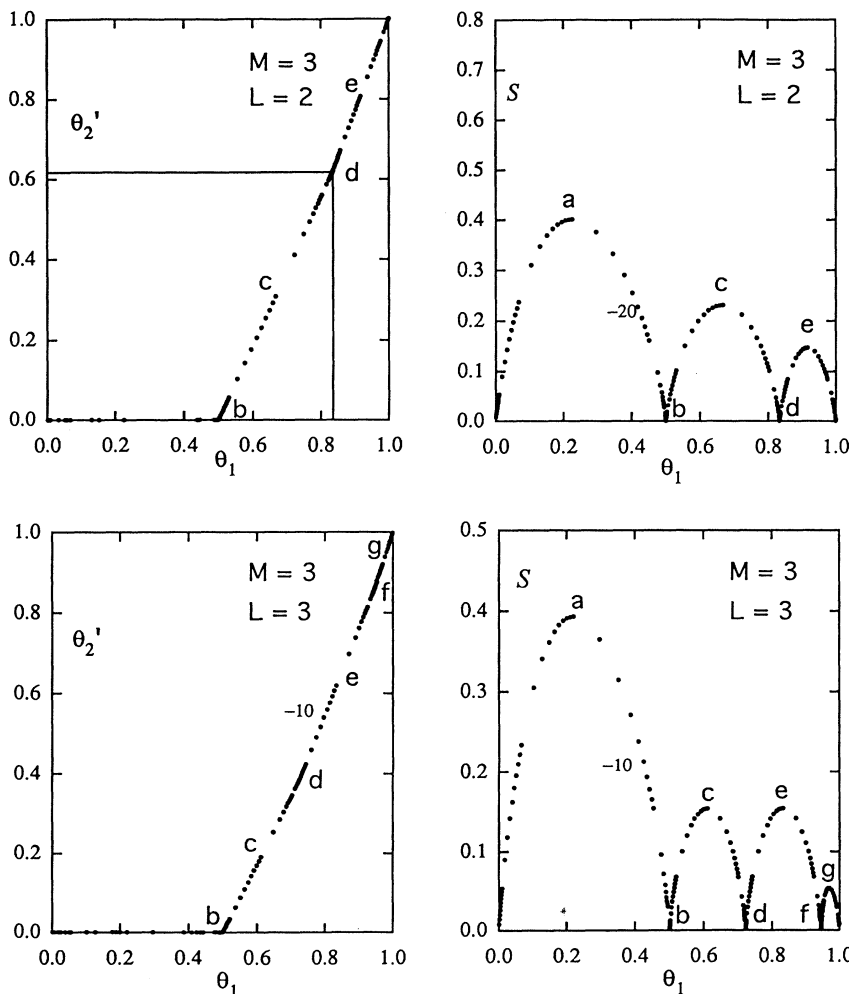


FIG. 4. Constant $\bar{\mu}_2$ curves of entropy $S$, and fraction of the maximum number of nearest neighbors $\theta_2'$ vs the coverage $\theta_1$, for $L = 2$, $M = 3$ and for $L = 3$, $M = 3$.

found in Table I. In particular, it is not surprising to find that the coverage at $c$ reaches $\frac{1}{2}$ (0.500 000 064 for $L=1$, 2, and 0.499 999 997 for $L=3$) in the limit of an infinite two-dimensional lattice for all three layers cases. In turn, this justifies the other linear extrapolations. The maximum at $a$ occurs when there are no nearest neighbors, and the maximum at $c$ merges with the two cusps $b$ and $d$ at $\frac{1}{2}$ coverage and no nearest neighbors. Figure 11 analyzes the fraction $\theta_2'$ of the maximum number of nearest neighbors at the remaining maxima, $e$ and $g$, and the results of the linear extrapolations are listed in Table I.

On the infinite two-dimensional lattice with one and two layers, our study confirms the progressive merging of the cusps into a single one occurring at $\theta_1=\frac{1}{2}$, $\theta_2=0$ as is the case in all Ising-type models. At sufficiently low temperature and large nearest-neighbor repulsion, the symmetry observed in one dimension of $S$ versus $\theta_1$ about $\theta_1=\frac{1}{2}$ appears to be preserved to better than 0.5%. This observation follows from the data listed in Table I and by comparing the properties at $a$ and $e$ for one and two layers. For the infinite lattice with three layers, no particu-



FIG. 6. Zero entropy monomer crystallization patterns on a semi-infinite two-layer lattice. The convention is the same as that adopted in Fig. 5. Here a section is made of two rows of $M$ sites.

lar symmetry is observed and we predict the existence of two cusps: at $\theta_1=\frac{1}{2}$, $\theta_2=0$; and at $\theta_1=\frac{5}{6}$, $\theta_2=\frac{5}{3}$. When including second neighbor repulsion between monomers, preliminary results show the existence of a cusp below $\frac{1}{2}$ coverage [9].

Having established the accuracy of linear extrapolations, Fig. 12 presents the coverage and entropy at $a$ for the infinite lattice with one, two, and three layers versus the reciprocal of the number of layers $(1/L)$. Linearity is again observed with the same accuracy as noted earlier. Linear extrapolation of the data to $(1/L)=0$ gives the values of the coverage and entropy at $a$ for the infinite three-dimensional lattice gas to be 0.2015 and 0.3605, respectively. This is in agreement with the series analysis result obtained by Gaunt for the simple cubic lattice [11], where his notation $\rho_t/\rho_0=2\theta_1$.
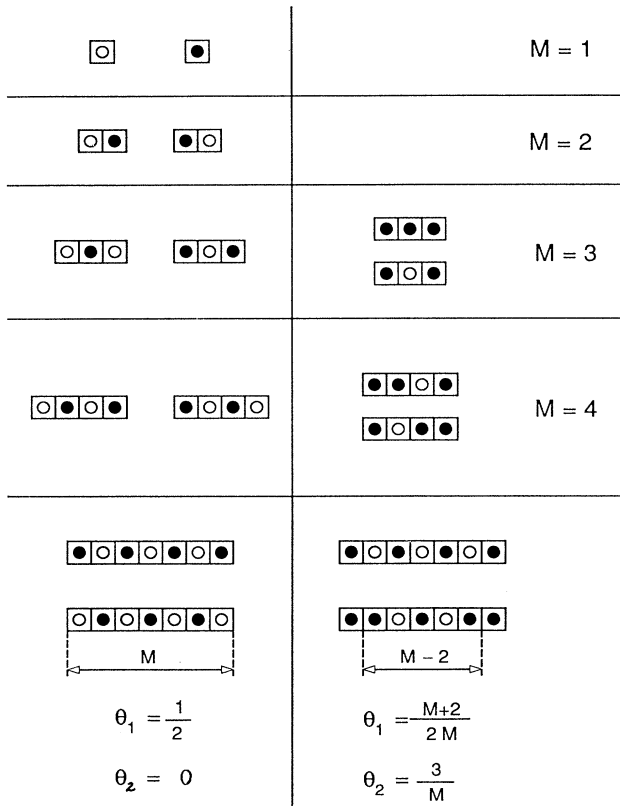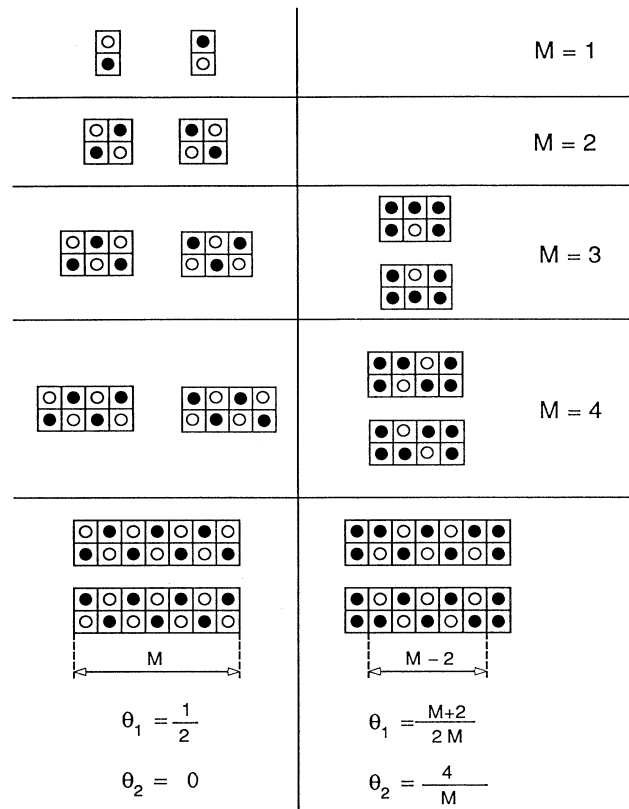


FIG. 5. Zero entropy monomer crystallization patterns on a semi-infinite one-layer lattice of width $M$. A lattice site is represented by a square cell, which has a circle when it is vacant, and a filled circle when it is occupied. Each set of diagrams represents the occupational configurations in any two consecutive sections of the lattice having $M$ sites.

## VI. ENERGY ANALYSIS

As mentioned earlier, an entropy curve at fixed activity $x_2$ is generated by varying the activity $x_1$. Since $\theta_2$ is observed to be an increasing function of $\theta_1$, and since Eq. (6b) must be satisfied at the maxima of the entropy, the

$$\theta_1 = \frac{1}{2} \qquad \theta_1 = \frac{3M+4}{6M} \qquad \theta_1 = \frac{5M+2}{6M}$$

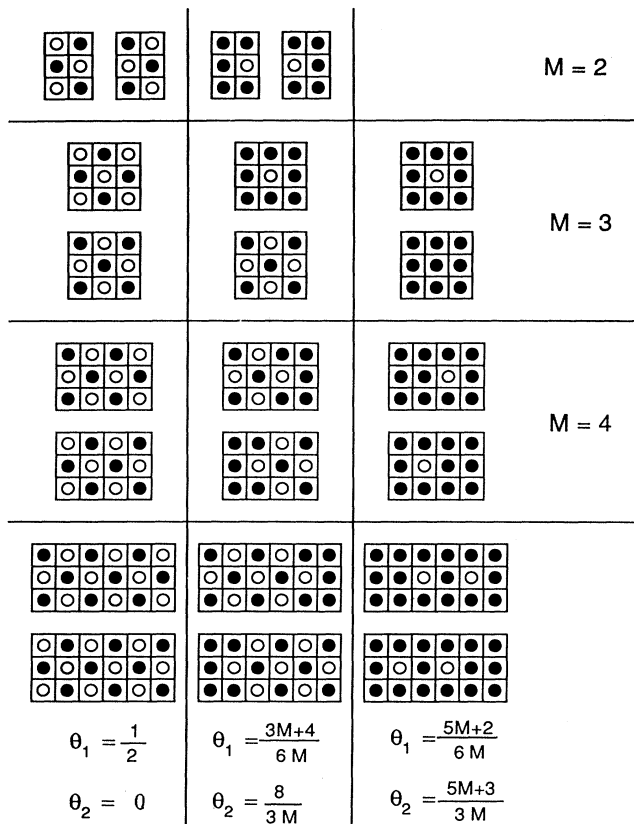$$\theta_2 = 0 \qquad \theta_2 = \frac{8}{3M} \qquad \theta_2 = \frac{5M+3}{3M}$$

FIG. 7. Zero entropy monomer crystallization patterns on a semi-infinite three-layer lattice. The convention is the same as that adopted in Fig. 5.

energy parameters $\bar{\mu}_1$ and $\bar{\mu}_2$ at these points must have opposite signs, and this is numerically verified. The data are for repulsive monomer-monomer interaction at sufficiently low temperature, and the corresponding points in the plot $\theta_2$ versus $\theta_1$ fall on the lower boundary of a polygon. The vertices of this lower boundary correspond to cusps in the entropy curve. Thus, we can compute the equations of the sides of the lower polygonal boundary from the knowledge of the cusp configurations listed in Figs. 5, 6, and 7. Two of the sides of the polygonal boundary are given by the equations

$$\theta_2' = \frac{LM}{3LM-L-M}\theta_2 = \theta_1, \quad \theta_2 = 0 . \tag{16}$$

The first equation is that of the upper boundary, and the second is that of one side of the lower boundary, from 0 to $\frac{1}{2}$ coverage. The remaining sides of the lower boundary have equations listed in Table II. The slopes of these boundaries are readily identified and, when substituted in Eq. (6b), give the exact interaction energy relations at the maxima, $a$, $c$, $e$, and $g$ of the entropy. These relations were numerically verified. Between a maximum and the following cusp, the chemical potential is larger than its value at that maximum, thus, just before a cusp [8],
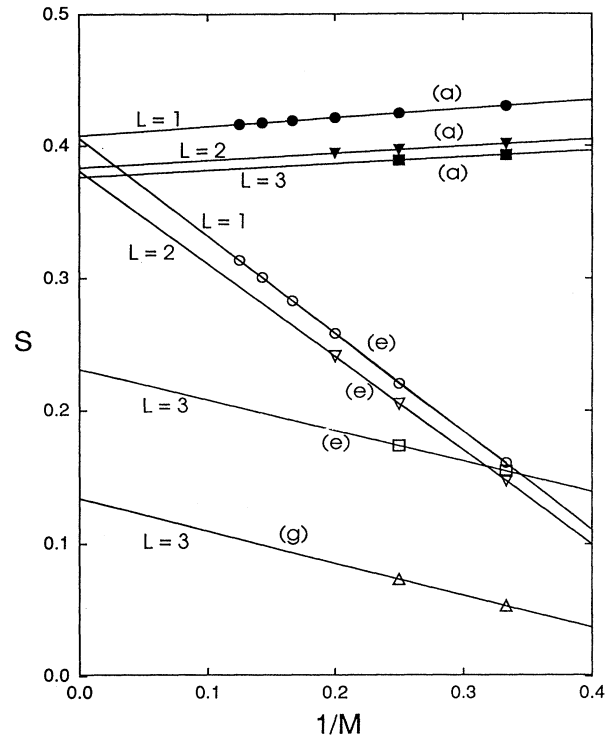


FIG. 8. Entropy vs the reciprocal of the lattice width for the maxima at $a$, $e$, and $g$ for one, two, and three layers.

$$\bar{\mu}_1 + \left[\frac{\partial\theta_2}{\partial\theta_1}\right]_{\text{before}} \bar{\mu}_2 = \beta > 0 , \tag{17}$$

where the label "before" refers to the slope of the boundary before the cusp. Just after this cusp, the chemical potential is less than its value at the next maximum, and,
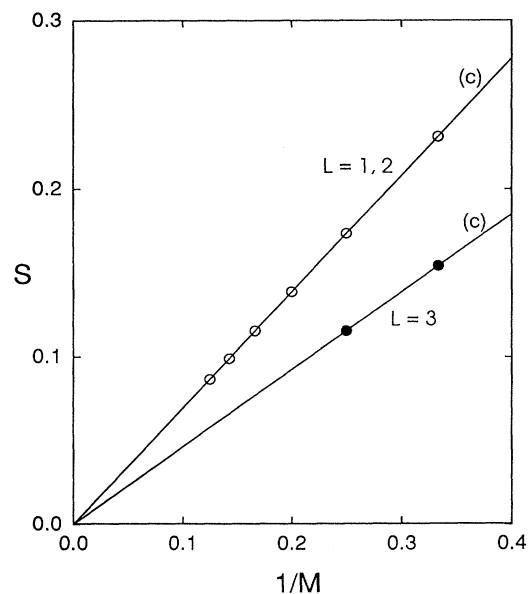


FIG. 9. Entropy vs the reciprocal of the lattice width at the maximum $c$ for one, two, and three layers.

TABLE I. Tabulation of the extrapolated entropy, coverage, and fraction of the maximum number of nearest neighbors, at points $a$, $e$, and $g$ (see Figs. 3 and 4), for infinite one, two, and three layers. Linear extrapolation to the infinite three-dimensional lattice is possible for $a$ only, and follows from Fig. 12. Note that, for the infinite one and two layers, the coverage at $a$ and $e$ are symmetrical with respect to $\frac{1}{2}$, and the respective entropies are within 0.5%.

| | | $a$ | | | $e$ | | | $g$ | |
| $L$ | $S$ | $\theta_1$ | $\theta_2'$ | $S$ | $\theta_1$ | $\theta_2'$ | $S$ | $\theta_1$ | $\theta_2'$ |
| --- | --- | --- | --- | --- | --- | --- | --- | --- | --- |
| 1 | 0.4075 | 0.2266 | 0 | 0.4051 | 0.7743 | 0.5517 | | | |
| 2 | 0.3835 | 0.2139 | 0 | 0.3813 | 0.7865 | 0.5308 | | | |
| 3 | 0.3765 | 0.2099 | 0 | 0.2310 | $\frac{2}{3}$ | 0.2808 | 0.1334 | 0.9255 | 0.8312 |
| $\infty$ | 0.3605 | 0.2015 | 0 | | | | | | |

therefore, in that region, we have [8]

$$\bar{\mu}_1 + \left[\frac{\partial\theta_2}{\partial\theta_1}\right]_{\text{after}} \bar{\mu}_2 = -\alpha < 0 \ , \tag{18}$$

where the label "after" refers to the slope of the boundary after the cusp. Since the entropy is exactly zero at the cusp, a departure from this value not exceeding, for example, 0.0001 automatically fixes the values of $\alpha$ and $\beta$, and the values of $\bar{\mu}_1$ just after and just before the cusp, respectively. Having made that choice, one obtains the amount of chemical potential energy change ($\Delta\bar{\mu}_1$), and the change in the external gas pressure, necessary to unlock the structural ordering for a given monomer species,

namely,

$$\Delta\bar{\mu}_1 + \left[\left[\frac{\partial\theta_2}{\partial\theta_1}\right]_{\text{after}} - \left[\frac{\partial\theta_2}{\partial\theta_1}\right]_{\text{before}}\right]\bar{\mu}_2 = -(\alpha+\beta) \ . \tag{19}$$

The slope *before* the first cusp is always zero. Table II shows that the difference between the slopes *after* and *before* the first cusp is 2, 3, or 4, depending on the width of the lattice and the number of layers. The difference between the slopes *after* and *before* a second or third cusp is one for all three layers. We use Eq. (1) and the numerical observation that crystallizations occur for $\bar{\mu}_2 < -5$ to obtain an estimate of the critical temperature $T_c$:

$$T_c \approx \frac{(-V_{11})\log_{10}(e)}{5k_B} \ . \tag{20}$$

For example, for a nearest-neighbor repulsion energy of 1 kcal/mole, the critical temperature is of the order of 44 K. With Eq. (1) and temperature $T < T_c$, Eq. (19)
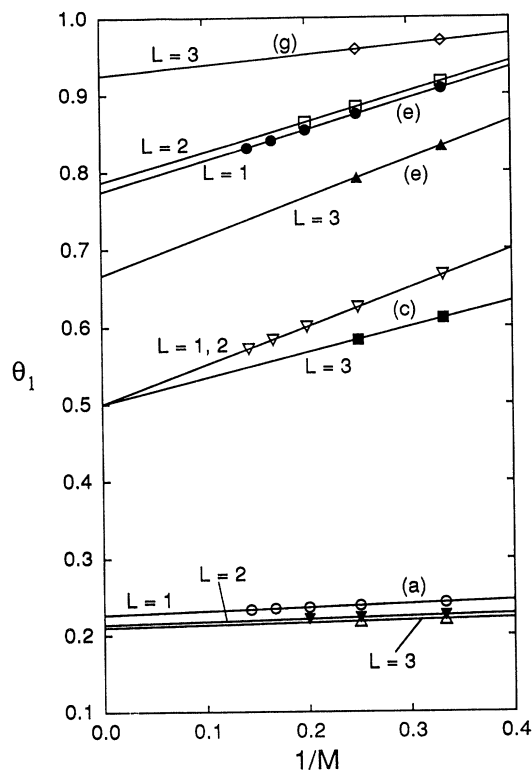


FIG. 10. Coverage of the lattice vs the reciprocal of the lattice width at the maxima of the entropy $a$, $c$, $e$, and $g$ for one, two, and three layers.
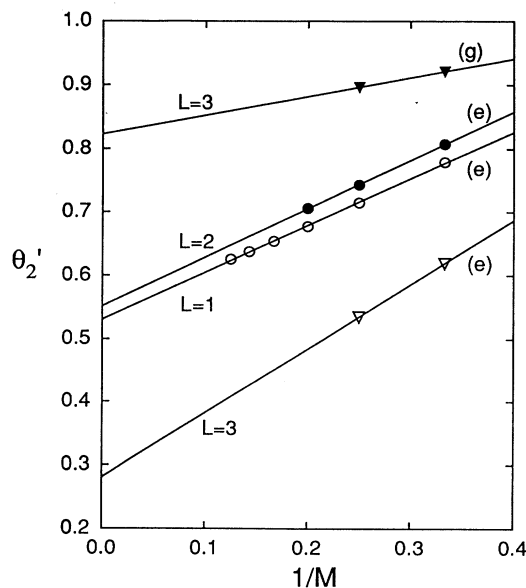


FIG. 11. Fraction of the maximum number of nearest neighbors vs the reciprocal of the lattice width at the maxima $e$ and $g$ of the entropy, for one, two, and three layers.

TABLE II. Equations of the polygonal boundary observed in the graph $\theta_2$ vs $\theta_1$ (see Figs. 3 and 4) corresponding to low temperature with monomer nearest-neighbor repulsion.

| Range $(M > 2)$ | $L = 1$ | $L = 2$ |
|---|---|---|
| $\dfrac{1}{2} \le \theta_1 \le \dfrac{M+2}{2M}$ | $\theta_2 = 3\theta_1 - \dfrac{3}{2}$ | $\theta_2 = 4\theta_1 - 2$ |
| $\dfrac{M+2}{2M} \le \theta_1 \le 1$ | $\theta_2 = 4\theta_1 - \dfrac{2M+1}{M}$ | $\theta_2 = 5\theta_1 - \dfrac{5M+2}{2M}$ |

| Range $(M > 2)$ | $L = 3$ |
|---|---|
| $\dfrac{1}{2} \le \theta_1 \le \dfrac{3M+4}{6M}$ | $\theta_2 = 4\theta_1 - 2$ |
| $\dfrac{3M+4}{6M} \le \theta_1 \le \dfrac{5M+2}{6M}$ | $\theta_2 = 5\theta_1 - \dfrac{15M+4}{6M}$ |
| $\dfrac{5M+2}{6M} \le \theta_1 \le 1$ | $\theta_2 = 6\theta_1 - \dfrac{10M+3}{3M}$ |

yields

$$\Delta\bar{\mu}_1 = C_1(-V_{11}) - C_2 T . \tag{21}$$

Here $C_1$ is 1, 2, 3, or 4 depending on the values of $L$ and $M$, as follows from the above analysis, and $C_2$ is a positive number depending on the conditions set to obtain $\alpha$ and $\beta$. Thus, at a temperature $T < T_c$, the change in the chemical potential necessary to unlock a structural ordering of the monomers is proportional to the nearest-neighbor repulsion energy, as verified numerically.
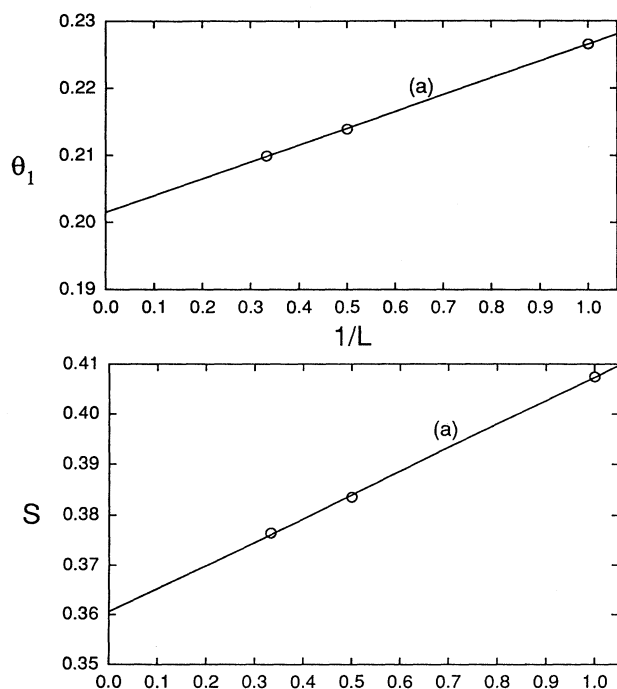


FIG. 12. Extrapolated coverage (top) and extrapolated entropy (bottom) at point $(a)$ vs the reciprocal of the number $L$ of infinite two-dimensional layers.

## VII. SUMMARY

The transfer matrix for the absorption of monomers on $L$ layers of a $M \times N$ square lattice, and with nearest-neighbor interaction, has been constructed recursively, and used to obtain the partition function. Some of the general features of the one-dimensional lattice are also found in the infinite two-dimensional lattice with one, two, and three layers. A theoretical study of the monomer structural ordering shows a series of zero entropy crystallization patterns occurring at low temperature for nearest-neighbor repulsion. The numerical computations not only verified these results, but also showed no other crystallization patterns, as opposed to the dimer lattice gas [8], where such patterns occur at nonzero entropy. At the crystallization points, as follows from Figs. 5, 6, and 7, the coverage, and the number of nearest neighbors per site are linear functions of $1/M$. Linearity at other points is accurate to better than five decimal places. The results of such linear extrapolations are listed in Table I. A second linear extrapolation of the numerical data plotted versus $1/L$, the reciprocal of the number of layers, appears to be possible only in the region $\theta_2 = 0$. This extrapolation provides the entropy and the coverage for the infinite three-dimensional lattice. These values were reported at point $a$, the first maximum of the entropy curve, to be 0.3605 and 0.2015, respectively.

The change in the chemical potential necessary to unlock the structural ordering below the estimated critical temperature is shown to be proportional to the nearest neighbor repulsion energy.

Work on the mixture of monomer and dimer species with nearest-neighbor interaction is in progress [9] with the intention of obtaining a model of chemical reactions on a surface.

## ACKNOWLEDGMENTS

[1] E. Ising, Z. Phys. **31**, 253 (1925).

[2] R. H. Fowler and E.A. Gugggenheim, *Statistical Thermodynamics* (Cambridge University Press, Cambridge, 1949); T. L. Hill, *Statistical Mechanics* (McGraw-Hill, New York, 1956); H. E. Stanley, *Introduction to Phase Transitions and Critical Phenomena* (Oxford University Press, New York, 1971); C. Domb, in *Phase Transitions and Critical Phenomena,* edited by C. Domb and M. S. Green (Academic, London, 1974), Vol. 2, Chap. 6, and other articles in this series; B. M. McCoy and T. T. Wu, *The Two-Dimensional Ising Model* (Harvard University Press, Cambridge, MA, 1973); R. J. Baxter, *Exactly Solved Models in Statistical Mechanics* (Academic, New York, 1982); J. W. Evans, Rev. Mod. Phys. **65**, 1281 (1993), and other references cited in this review article.

[3] R. H. Fowler and G. S. Rushbrooke, Trans. Faraday Soc. **33**, 1272 (1937).

[4] H. A. Kramers and G. H. Wannier, Phys. Rev. **60**, 252 (1941); **60**, 263 (1941).

[5] D. S. Gaunt and M. E. Fisher, J. Chem. Phys. **43**, 2840 (1965); L. K. Runnels and L. L. Combs, Phys. Rev. **45**, 2482 (1966); F. H. Ree and D. A. Chesnut, *ibid.* **45**, 3983 (1966).

[6] J. L. Hock and R. B. McQuistan, J. Chem. Phys. **89**, 2292 (1988).

[7] C. N. Yang and T. D. Lee, Phys. Rev. **87**, 404 (1952); M. E. Fisher, Rep. Prog. Phys. **30**, 615 (1967).

[8] A. J. Phares, F. J. Wunderlich, J. W. Grumbine, Jr., and J. D. Curley, Phys. Lett. A **173**, 365 (1993); A. J. Phares, F. J. Wunderlich, J. D. Curley, and D. W. Grumbine, Jr., J. Phys. A **26**, 6847 (1993).

[9] A. J. Phares and F. J. Wunderlich (unpublished).

[10] See, for example, *The Chemical Physics of Solid Surfaces,* edited by D. A. King and D. P. Woodruff (Elsevier, Amsterdam, 1993), Vol. 6.

[11] D. S. Gaunt, J. Chem. Phys. **46**, 3237 (1967), Eq. (4.38).